

Negative differential resistances pinned by kink effect in graphene double barrier resonant tunneling diodes

Yu Song,^{1,*} Han-Chun Wu,² and Yong Guo¹

¹*State Key Laboratory of Low-Dimensional Quantum Physics and Department of Physics, Tsinghua University, Beijing 100084, People's Republic of China*

²*CRANN and School of Physics, Trinity College Dublin, Dublin 2, Ireland*

(Dated: October 9, 2012)

We theoretically investigate negative differential resistance (NDR) in graphene double barrier resonant tunneling diodes within the Landauer-Büttiker formalism by considering a realistic linear voltage drop. The calculated current-voltage characteristic indicates that, due to the competition between hole-to-electron transport, Klein paradox, and resonant tunneling, the NDR is substantially suppressed and only presents for appropriate structural parameters. Remarkably, the first NDR operation window is always pinned by a robust kink effect to around the Fermi energy, which may open an interesting window for designing NDR based graphene devices in a controllable way. Moreover, the peak-to-valley current ratio can be enhanced epitaxially and parabolically by opening a band gap and adjusting structural asymmetries, respectively.

I. INTRODUCTION

The negative differential resistance (NDR) is a fundamental phenomenon in physics and can be utilized to generate bistable switching circuits and electronic oscillators [1]. It has been observed in various systems, ranging from gaseous medium [2] via chalcogenide glasses [3] to organic semiconductors [4] and conductive polymers [5]. Recently, significant efforts [6–16] have been devoted to the study of NDR in graphene, a monolayer of sp^2 bonded carbon atoms that has attracted much attentions since its discovery [17]. Besides its occurrence in graphene single barrier diodes (SBDs) [6–8], the NDR has also been theoretically reported in zigzag graphene nanoribbons [9], armchair graphene nanoribbons [10, 11], and numerous graphene nanoribbon junctions [12–14], governed by the mechanisms of chiral selective tunneling, electrodes doping or strain, and suppression of the coherent transition, respectively. Very recently, it is suggested that the NDR can be obtained in armchair graphene superlattices [15] by band gaps, miniband conductance, and Wannier-Stark ladder and rather surprisingly in graphene three terminal field-effect transistors [16] by just considering classical ambipolar transport.

It is well-known that Fabry-Pérot-type interference is an alternatively fundamental mechanism for NDR and plays a dominant role on the NDR in common semiconductor based resonant tunneling diodes (RTDs) [18]. Surprisingly, this mechanism has not been explored in graphene so far except a rather recent study on *semi-conducting* armchair graphene nanoribbon *superlattices* [15] in which, however, other mechanisms as mentioned above also contribute to the NDR features thus significantly obscure the resonant tunneling mechanism. On the other hand, in those above works based on analytic models [6–8, 15] the voltage drop produced by the bias

has been approximated by a steplike one of the average value. (See, Figs. 1, 3, and 1 in Refs. [6], [8], and [15], respectively.) This approximation greatly simplifies the calculations (see below), but actually describes a bias-dependent nonequilibrium barrier which may draw a false conclusion of the NDR feature.

In present work, we for the first time consider a realistic linear voltage drop and investigate the NDR in graphene double barrier (DB) RTDs. The said DB RTDs can be fabricated by patterning two top gates [19] on a short and sufficient wide graphene strip [20], thus the edge effect can be ignored and the NDR feature solely relies on the resonant tunneling mechanism. To investigate the I-V characteristic, we analytically solve the envelope wave functions in a rotated pseudospin space. We find that the NDR in graphene DB RTDs has been substantially suppressed comparing with that in common semiconductors, and it only appears with appropriate structural parameters. We attribute such a suppression to hole-to-electron transport and the Klein paradox, and propose a way to enhance the strength of NDR (defined as the peak-to-valley current ratio (PVR)) by introducing a band gap in the linear dispersion of graphene or adjusting the structural parameters. Remarkably, our calculations show that the NDR is pinned by a so-called kink effect and the first operation window always appears around the Fermi energy [21]. This phenomenon has not been found in other type NDR devices and may provide an interesting opportunity for designing and utilizing NDR based devices in a controllable way. Moreover, our results also indicate that the NDR is absent in graphene SBDs as long as the linear voltage drop is taken into account.

The paper is organized as follows. In Sec. II we introduce the theoretical model and formula that we use in order to calculate the I-V curves. In Sec. III we present the I-V and DC characteristics for graphene SBDs concerning the linear voltage drop. In Sec. IV we exhibit the kink-effect pinning NDR in graphene DB RTDs and in Sec. V we investigate the role of band gaps and struc-

* kwungyusung@gmail.com

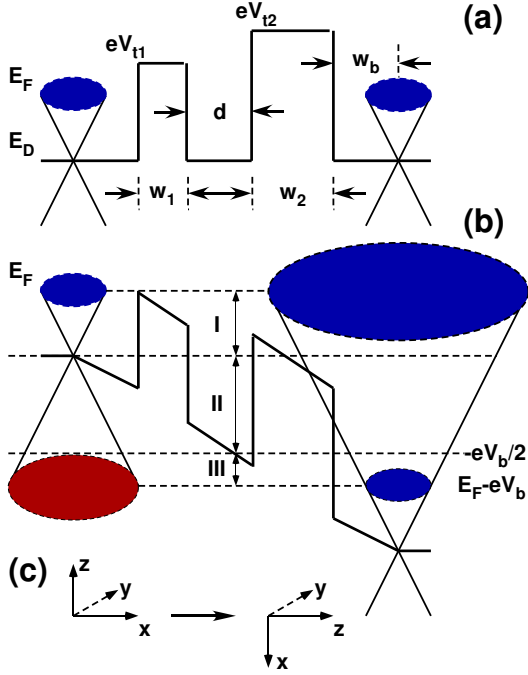


FIG. 1. (color online) Model construction for I-V characteristic of a graphene DB RTD, under (a) no bias and (b) a finite bias V_b . The diode contains a buffer (width w_b), two barriers (width $w_{1(2)}$ and height $V_{t1(2)}$), and a well (width d) regions. For (b) a linear voltage drop appears and the transport can be divided into three regimes (I, II, and III) defined by E_F and V_b . (c) The rotation we make in the pseudospin space.

tural asymmetries on the NDR strength. A summary will be given in Sec. VI.

II. MODEL AND FORMULA

Fig. 1(a) shows a schematic of a graphene DB RTD under zero bias. To investigate its intrinsic I-V characteristic, we restrict our study to the ideal contacts case which in practice can be achieved by using a high- κ (dielectric constant) material as electrodes [22]. The contact resistance and the doping effect by electrodes then can be ignored. The Fermi energy E_F (relative to the Dirac point $E_D \equiv 0$) and the carrier concentration ($\propto |E_F|$) [17] in the stripe are tuned by a back gate voltage. The potential barriers ($V_{t1(2)}$) can be formed by top gates [19]. We adopt rectangular potential barriers, since smooth barriers considering the electric field on the interfaces can be regarded as rectangular ones with the same widths but effective heights determined by the smoothness [23]. As sketched in Fig. 1(b), when a bias voltage (V_b) is applied, a linear voltage drop will be formed between the two electrodes due to a uniform electric field and a net current will be produced by the holes or electrons with energies $E \in [E_F - eV_b, E_F]$. The charge transport can be classified into three regimes depending on the values of E_F and V_b as denoted in Fig.

1(b). In regime I ($0 < E < E_F$), it is electron-to-electron transport; while in both regimes II ($-eV_b/2 < E < 0$) and III ($E_F - eV_b < E < -eV_b/2$), it is hole-to-electron transport. The difference between the latter two regimes is that in regime III only holes from the left electrode within critical incident angles $\mp \sin^{-1}(1 + eV_b/E)$ can transport to electrons in the right electrode. One can see that when $eV_b < E_F$, only regime I is possible; when $E_F < eV_b < 2E_F$, regime II is also present; while for $eV_b > 2E_F$ all these three regimes make contributions to the net current.

At 0K the net current under a bias V_b can be given by the Landauer-Büttiker formalism [24]

$$I(V_b) = I_0 \int_{\epsilon_F - v_b}^{\epsilon_F} \int_{-\pi/2}^{\pi/2} T(\epsilon, \theta, v_b) |\epsilon| \cos \theta d\theta d\epsilon, \quad (1)$$

where $I_0 = 4ev_F W_y / (2\pi d_0)^2$ is a current unit. The factor 4 comes from the spin and valley degeneracies, $v_F \approx 10^6 m/s$ is the Fermi velocity, and W_y is the width of the graphene strip. d_0 is a characteristic length of the structure which is adopted as 40 nm to ensure the electron density of states coinciding with a true system and a coherent transport regime at room temperature. E_F and V_b in the integral are written in the dimensionless form; see the next paragraph for details. To obtain the value of the current, one needs to calculate the transmission probabilities (T) at $E \in [E_F - eV_b, E_F]$ first. This can be obtained by matching spinor wavefunctions ($\Psi(x, y)$) in different regions at potential boundaries to ensure the conservation of the local current density ($\mathbf{j}(\mathbf{r}) = 4ev_F \Psi^\dagger(\mathbf{r}) \boldsymbol{\sigma} \Psi(\mathbf{r})$). However, direct derivations from the Dirac equation with a horizontal electric field result in an unsolvable two-order differential equation. In Refs. [6–8, 15] this dilemma has been circumvented by approximating the linear voltage drop with an average value. However, such an approximation describes a nonequilibrium barrier which may induce a nonphysical current.

Here, we perform a rotation of the Dirac equation by $\pi/2$ around the y -axis in the pseudospin space (see, Fig. 1(c)). After rotation the Hamiltonian becomes

$$H = v_F [\sigma_z (p_x + eA_x) + \sigma_y (p_y + eA_y) - \sigma_x \Delta] + eV(x) \mathbf{I}, \quad (2)$$

and the two components of the spinor (ψ^\pm) relate to the ones before rotation ($\psi^{\uparrow\downarrow}$) by $\psi^\pm = (\pm\psi^\uparrow + \psi^\downarrow)/\sqrt{2}$. Here $\psi^{\uparrow\downarrow}(x, y)$ is the envelope function at sublattice site A/B of the graphene sheet, $\boldsymbol{\sigma} = (\sigma_x, \sigma_y, \sigma_z)$ are Pauli's matrices, \mathbf{I} is the 2×2 identity matrix, $\mathbf{p} = (p_x, p_y)^T = (\hbar k_x, \hbar k_y)^T$ is the momentum operator, $\mathbf{A} = (A_x, A_y)^T$ is a possible magnetic vector potential, Δ is a tunable band gap up to several hundreds of meV achieved through a controllable doping [25], and $V(x)$ is the position dependent electrostatic potential. In terms of d_0 all these parameters can be expressed in a dimensionless form: $x = x/d_0$, $k = kd_0$, $\epsilon = E/E_0$, $\delta = \Delta/E_0$, and $v(x) = eV(x)/E_0$ with an energy unit $E_0 \equiv \hbar v_F/d_0 \approx 16.44$ meV.

From Eq. (2) we get coupled one-order differential equations $[i\partial/\partial x \pm (\epsilon - v(x))]\psi^\pm = (-\partial/\partial y \mp \delta)\psi^\mp$. Taking into account solutions of $\psi^\pm(x, y) = f^\pm(x)e^{ik_y y}$ due to the translation invariance in the y -axis, we get a decoupled two-order differential equation

$$\left\{ \frac{d^2}{dx^2} \pm i \left[\frac{d}{dx}, v(x) \right] + [\epsilon - v(x)]^2 - q^2 \right\} f^\pm(x) = 0, \quad (3)$$

where $[d/dx, v(x)]$ is a commutator due to the noncommutativity of \hat{p}_x and \hat{x} [26] and $q^2 = k_y^2 + \delta^2$. In the electrode regions ($v(x) = \text{const}$), this equation recovers the one before performing rotation, $[d^2/dx^2 + (\epsilon - v)^2 - q^2]f^\pm(x) = 0$. The direct wave function solutions from this equation should be composed as mentioned above. In the buffer and well (barrier) regions, $v(x) = -ax(+v_t)$, where $a = eV_b/L$ and L is the total width between the electrodes. Now, the wave functions of Eq. (3) can be solved as

$$\Psi = p \begin{pmatrix} F \\ G \end{pmatrix} + q \begin{pmatrix} G^* \\ F^* \end{pmatrix}, \quad (4)$$

where $F = D[-1 + iq^2/2a, (1+i)(\epsilon + ax(-v_t))/\sqrt{a}]$, $G = (1+i)\sqrt{a}q^{-1}D[iq^2/2a, (1+i)(\epsilon + ax(-v_t))/\sqrt{a}]$, and the superscript stands for complex conjugate. Here D is the Weber parabolic cylinder function. F and G have properties of a right-going wave function as the amplitude of the classical trajectory at the right turning point (the points where $k_x(x) = \sqrt{(\epsilon - v(x))^2 - q^2}$ becomes zero) is about $e^{-\pi q^2/a}$ times of that at the left turning point. Since we have got wave functions in the electrodes and intermediate regions, we can obtain the transmission coefficient (t) by the standard transfer-matrix method [27]. The transmission probability reads $T = \frac{k_{xR}/(\epsilon + v_b + \delta)}{k_{xL}/(\epsilon + \delta)} |t|^2$ for $k_{xL}^2 > 0$ and $k_{xR}^2 > 0$, and $T = 0$ otherwise, where $k_{xL(R)}$ is the value of k_x at the left (right) electrode. Then the current can be calculated by Eq. (1).

III. I-V CHARACTERISTIC IN GRAPHENE SBDS

To evaluate the results taking into account a realistic linear voltage drop, and more importantly, to obtain a basic picture for biased transport in graphene in absence of resonant tunneling, we'd like to revisit the NDR in graphene SBDs first. Fig. 2 shows the I-V and differential conductance (DC) curves for a graphene SBD with $w_b = 1$, $w = 1$, and $v_t = 2$ at various back gate voltages. As is seen, for zero back gate (i.e., $E_F = 0$), the I-V curve is superlinear ($I \propto V_b^2$) for $V_b < V_t$ and nearly linear ($I \propto V_b$) for $V_b > V_t$. This is a result of that the current is totally due to the hole-to-electron Zener-Klein tunneling. As long as the Fermi energy is lifted, the DC displays totally different behaviors in the three transport regimes (see, Fig. 2(b)). Take $\epsilon_F = 1$ (black dotted line) as an example. In regime I, the DC decreases with increasing V_b and reaches G_m exactly at $eV_b = E_F$. This is

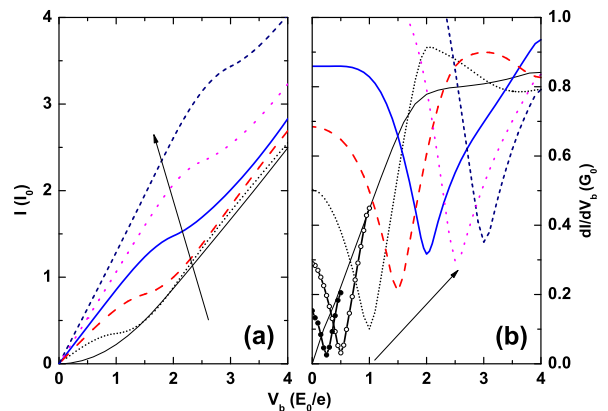


FIG. 2. (color online) (a) I-V and (b) DC characteristics for a graphene SBD with parameters of $w_b = 1$, $w = 1$, $v_t = 2$. Along the arrow, $\epsilon_F = 0, 1, 1.5, 2, 2.5$, and 3 , respectively. In (b) the DC is also shown for $\epsilon_F = 0.25$ (line with dots) and 0.5 (line with circles) in small ranges. The conductance unit is $G_0 = 4e^2 W_y / 2\pi \hbar d_0$.

because the bias-induced electron concentration (approximately $\propto E - eV_b$) which contributes to the DC decreases with the bias. Further increasing eV_b to $2E_F$ (regime II), the DC increases with increasing V_b and reaches a maximum at $V_b = 2E_F$. In this regime, the bias-induced hole concentration (approximately $\propto eV_b - E$) increases with bias. When eV_b exceeds $2E_F$ (regime III), increasing bias will increase the hole concentration but decrease the DC as only holes with incident angles smaller than the critical value contribute to the transport. As a result of such an ambipolar transport by both electron and hole, the I-V curve shows a *kink effect* exactly at $eV_b = E_F$, which has been observed by recent experiments [28].

Interestingly, G_m increases with increasing E_F (the $\epsilon_F = 2$ case is an exception maybe due to it equals exactly to the barrier potential) and is positive even for a rather small E_F . In other words, there is no NDR effect in graphene-based SBDs. This conclusion is in strong contrast to the one obtained by Dragomans [6] and Nam Do *et al.* [7, 8]. The artificial current induced by the steplike voltage drop in their works may be responsible for the announced NDR effect. Note, the reduction in T may give rise to NDR in SBDs based on common semiconductors (such as $\text{Hg}_{1-x}\text{Cd}_x\text{Te}/\text{CdTe}$ [29] and $\text{AlGaSb}/\text{InAs}$ [30]). Here the situation substantially changes for graphene. Due to the transport regimes II and III which are absent in common semiconductor cases, the number of tunneling carriers (both electrons and holes) increase rather than saturate with increasing bias. Then the reduction in T is obscured and the NDR effect is absent in graphene SBDs.

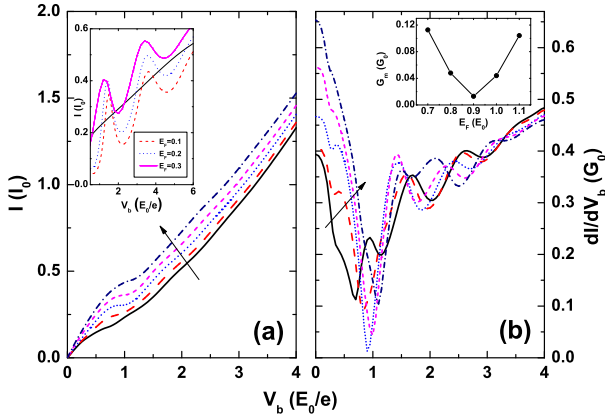


FIG. 3. (color online) (a) I-V and (b) DC characteristics for a graphene DB RTD with parameters of $w_b = 1$, $w_{1(2)} = 1$, $d = 5$, and $v_{t1(2)} = 1$. Along the arrow, $\epsilon_F = 0.7, 0.8, 0.9, 1.0$, and 1.1 . Insert in (a): I-V characteristic for a 2DEG DB RTD with the same parameters (note now $E_0 = \hbar^2/2md_0^2$ with m the electron mass in 2DEG). The thin line shows I-V characteristic for a 2DEG SBD with $E_F = 0.2E_0$. Insert in (b): the minimum DC as a function of the Fermi energy.

IV. NDR IN GRAPHENE DB RTDS

We now seek NDR in graphene DB RTDs and investigate its correlation with the resonant tunneling. Fig. 3 shows the I-V and DC characteristics for a graphene DB RTD with $w_b = 1$, $w_1 = w_2 = 1$, $d = 5$, and $v_{t1} = v_{t2} = 1$ at various back gating. While exhibiting similar trend as the ones for a graphene SBD, the I-V curves here for a graphene DB RTD display obvious ripples and correspondingly the DC oscillates with the bias. This is a result of the alternate enhancement and suppression of T respectively around and between resonant tunnelings (see, Fig. 4(a)). For the latter case, the DC reaches local minimums G_{lm} at some biases. One can see from Fig. 3(b) that at biases sufficiently low or high compared with the Fermi energies, G_{lm} moves to a lower bias for a higher Fermi energy (see, the groups around $v_b = 0.2, 1.7$, and 2.8 ; the one around $v_b = 1.2$ for $\epsilon_F = 0.7$ is excluded in this analysis). However, the lowest G_{lm} (i.e., G_m) always locates exactly at $eV_b = E_F$. It first decreases with increasing E_F until reaching the minimum DC of the structure, and then increases with increasing E_F (see, insert in Fig. 3(b)). Note, the minimum DC of the structure depends only on the structural parameters and for the considered structure, the minimum DC appears at $E_F = 0.9$. In total, the G_m is always positive, which means that there is no NDR in such a graphene DB RTD.

This is an interesting conclusion since the NDR always occurs for common semiconductor based DB RTDs (see inset in Fig. 3(a)). It is well known that in the semiconductor RTDs, NDR occurs when the suppression region

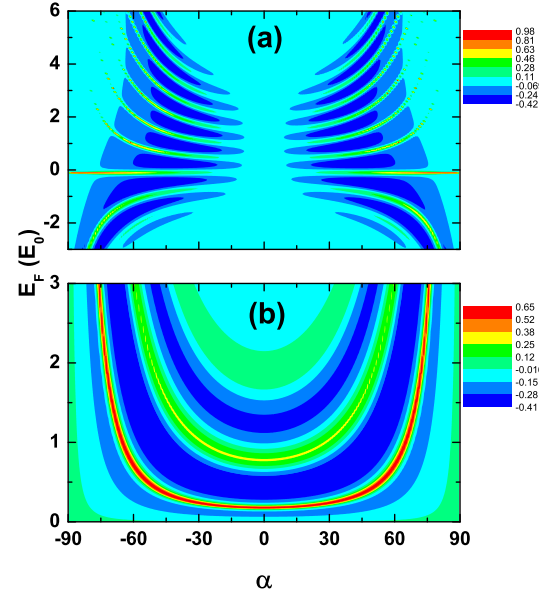


FIG. 4. (color online) Difference of transmission probabilities between a unbiased DB RTD and constituted single barrier for (a) graphene and (b) 2DEG with the same parameters of $w_{1(2)} = 1$, $d = 5$, and $v_{t1(2)} = 1$.

of T between two adjacent resonant tunneling peaks (i.e., blue regions in Fig. 4(b)) enters the integration window $[E_F - eV_b, E_F]$ of the current [18]. Meanwhile, one can see from Eq. (1) that the contribution of the suppression regions to the NDR mainly comes from ones near $\theta = 0$ due to the $\cos\theta$ factor. However, in graphene these regions are significantly reduced. Due to the Klein paradox, the suppression region between quasibound states (equivalently, resonant tunnelings) cannot form especially for small incident angles (see, Fig. 4(a)). Moreover, as indicated in the above graphene SBD calculations, when eV_b exceeds E_F the hole-to-electron tunneling contributes a positive DC (which increases with increasing bias) hence suppresses the NDR feature in graphene. Therefore, the NDR effect in graphene DB RTDs is a competition between hole-to-electron transport, Klein paradox, and resonant tunneling.

Our calculations further indicate that, the absence of NDR can be overcome by enhancing the resonant tunneling with more appropriate structural parameters. Specifically, the less the number of quasibound states (which approximately equals to the value of $v_t d$), the stronger the contribution of the resonant tunneling. Fig. 5 shows the results for a structure of $w_b = 1/2$, $w_1 = w_2 = 1/2$, $d = 1/2$, and $v_{t1} = v_{t2} = 2$. One can see that G_m becomes negative for $\epsilon_F \approx 2.6 - 3.2$. Therefore the NDR can be obtained in graphene DB RTDs with proper structural parameters. It is noted in Fig. 5(b) that, even in the presence of NDR feature, G_m is also locked exactly at

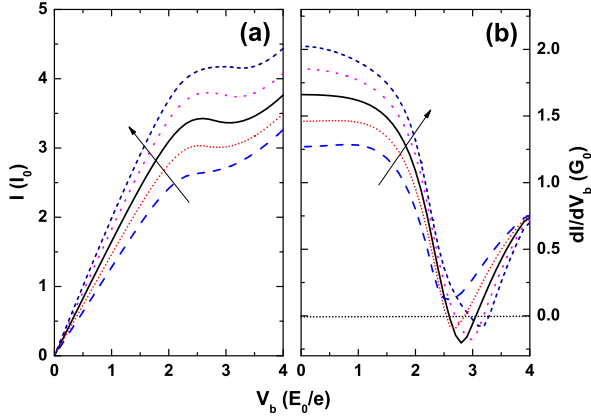


FIG. 5. (color online) (a) I-V and (b) DC characteristics for a graphene DBD with parameters of $w_b = 1/2$, $w_{1(2)} = 1/2$, $d = 1/2$, and $v_{t1(2)} = 2$. Along the arrow, $\epsilon_F = 2.4, 2.6, 2.8, 3.0$, and 3.2 .

$eV_b = E_F$, implying that the kink effect is robust against the resonant tunneling. This means that the first NDR operation window can be chosen or tuned easily by a single parameter, i.e., the Fermi energy.

V. EFFECT OF BAND GAPS AND STRUCTURAL ASYMMETRIES

However, the value of PVR is rather small (about 1.02 for the strongest case $\epsilon_F = 2.8$) for these symmetry structures based on gapless graphene. Fig. 6(a) shows the I-V characteristic for a graphene DB RTD with different band gaps. As is seen, when there is an induced band gap in graphene (which should be restricted to not exceed the value of Fermi energy), the current decreases for any given bias. This is a result of the reduction of number of electron/holes from the left electrode (i.e., the ones with $|\epsilon \cos \theta| < \delta$ cannot propagate freely) and the suppression of T by the band gap. When the band gap is sufficiently large (say $\delta \geq 1.5$), the I-V characteristic at low bias region even becomes superlinear and a second NDR operation window with a much weaker strength appears at higher bias (see, Figs. 7 and 8). However, the PVR for the first operation window does increase with increase δ (see, Fig. 6(b)). The increase follows an exponential function of the band gap ($\text{PVR} \approx 0.9832 + 0.0413e^{1.29\delta}$ for the considered case). The underlying physics is that, the presence of band gap increases the modulus of the image longitudinal wave vector in the barriers ($\kappa_x(x) = [\delta^2 + k_y^2 - (\epsilon - v(x))^2]^{-1/2}$), which makes a stronger suppression of T between adjacent resonant tunnelings hence results in a bigger PVR.

We now study the effect of the structural asymmetries of DB RTDs, i.e., the two potential barriers have different widths and/or heights. To give a quantitative

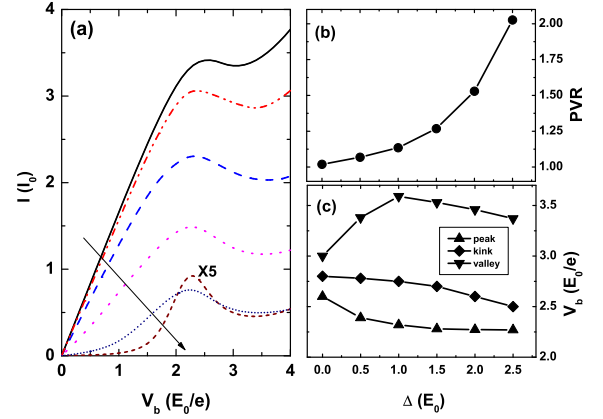


FIG. 6. (color online) (a) I-V characteristics for the graphene DB RTD considered in Fig. 5 with different band gaps. Along the arrow, $\Delta/E_0 = 0, 0.5, 1.0, 1.5, 2.0$, and 2.5 (enlarged by 5 times for clearness). (b) The peak-to-valley current ratio and (c) the biases for the current peak, kink, and valley points as a function of the induced gap.

evaluation, here we suppose that the height of the left (right) barrier is lower (higher) than a referenced symmetric one by a ratio of $\lambda_h \equiv (v_t - v_{t1})/v_t = (v_{t2} - v_t)/v_t$, which can be defined as an asymmetry degree in barrier heights (ADBH). Fig. 7(a) shows I-V characteristics for graphene DB RTDs with different ADBHs and corresponding PVR's and biases for the peaks, kinks, and valleys are plotted in Fig. 7(b) and 7(c), respectively. As is seen, the I-V curves exhibit regular variations with increasing ADBH, not only in gradually decreasing bias positions for the peak, kink, and valley but also in a parabolic-like ADBH dependent PVR. The maximum PVR is achieved at about $\lambda_h = 0.2$ (i.e., $v_{t1}:v_{t2}=2:3$). Note, $\lambda_h = 0$ stands for a symmetric DB RTD, for which the resonant tunneling does not achieve the optimal one under bias [31]; while $\lambda_h = 1$ means actually a single barrier diode, for which the NDR never happen as we have shown in Section II. This qualitatively explains why the maximum PVR happens at an intermediate ADBH between 0 and 1.

Fig. 8(a) shows I-V curves for different asymmetry degrees in barrier widths (ADBWs), which are similarly defined as $\lambda_w \equiv (w - w_1)/w = (w_2 - w)/w$. It is seen that, the low bias behaviors almost coincide no matter how big the ADBW is. Different from the changes due to asymmetry in barrier heights, where all the biases for the peak, kink, and valley decrease with increasing ADBH, here the biases for the peak and kink increase slightly with increasing ADBW, while the one for the valley shows a weak parabolic-like behavior (see, Fig. 8(c)). More importantly, the PVR also shows a parabolic-like dependence on the ADBW with the maximum also at about $\lambda_w = 0.2$ ($w_1:w_2=2:3$) (see, Fig. 8(b)). This similarity in the PVR behaviors implies the similar effects of asymmetries in barrier heights and widths. Further

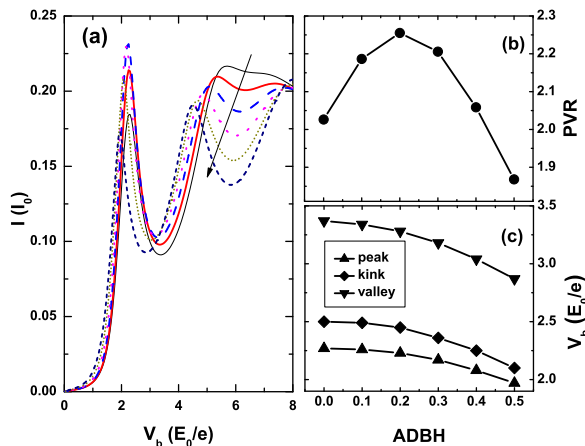


FIG. 7. (color online) (a) I-V characteristics for the graphene DB RTD considered in Fig. 5 with $\delta = 2.5$ and different ADBHs. Along the arrow, $\lambda_h=0, 0.1, 0.2, 0.3, 0.4$, and 0.5 . (b) The peak-to-valley current ratio and (c) the biases for the current peak, kink, and valley points as a function of λ_h .

calculations show that bigger PVRs can also be achieved by a joint of both asymmetries of heights and widths. However, the effect for a value of $\lambda_h + \lambda_w$ is somewhat the same for a same value of an individual λ_h or λ_w . The different dependencies of PVR on band gap and ADBH or ADBW come from that the band gap not only suppresses hole-to-electron transport and Klein paradox but also enhances resonant tunneling, while the structural asymmetries only enhance resonant tunneling in a proper range.

In Sec. IV, we have seen that the first NDR operation window is pinned by the kink effect. Now Figs. 6(c)-8(c) tell us that, the kink effect is also robust against the band gaps or structural asymmetries. As a result, even with these factors, the first NDR operation window can be solely determined by the Fermi energy. This is a totally new feature for NDR in graphene that has not been found in any other types of graphene NDR devices.

VI. CONCLUSIONS AND REMARKS

In summary, we have constructed an analytic model which takes into account the realistic linear voltage drop and three transport regimes to investigate the NDR effect of massless Dirac Fermions in graphene DB RTDs. The I-V and DC characteristics are calculated within the Landauer-Büttiker formalism in the rotated pseudospin space. The results indicate that, in graphene DB RTDs the NDR is a result of competition between hole-to-electron transport, Klein paradox, and resonant tunneling, and it only presents for appropriate structural

parameters. We have also proposed a way to enhance

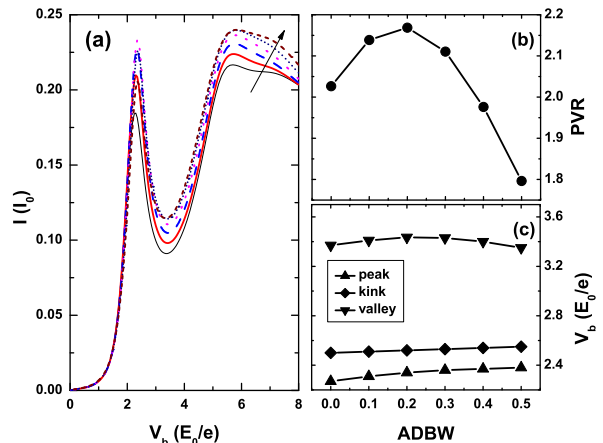


FIG. 8. (color online) (a) I-V characteristics for the graphene DB RTD considered in Fig. 5 with $\delta = 2.5$ and different ADBWs. Along the arrow, $\lambda_w=0, 0.1, 0.2, 0.3, 0.4$, and 0.5 . (b) The peak-to-valley current ratio and (c) the biases for the current peak, kink, and valley points as a function of λ_w .

the NDR strength by a tunable band gap in graphene and structural asymmetries of the DB RTD and investigated their roles on the PVR. Our results show that the PVR can be enhanced near exponentially by the induced band gap while it displays a parabolic-like dependence on the asymmetric degree in barrier heights and/or widths. We also observe a totally new and remarkable feature: the operation window of NDR in graphene DB RTDs is always pinned by a robust kink effect hence can be controlled easily by solely tuning the Fermi energy. This fact provides an opportunity for designing NDR based devices, such as high-speed bistable switching circuits and very high frequency oscillators, in a controllable way.

Our calculations also show that the differential conductance displays totally different behaviors in the three transport regimes, and moreover, the NDR is absent in graphene SBDs which is in contrast to the earlier reports. Noting that the NDR only occurs in DB RTD with proper parameters, it is not surprising that the NDR never occurs in SBDs where no resonant tunneling takes place. Although we take graphene as an example, the results also apply to surface states of 3D topological insulators [32] where the real electron spin rather than the sublattice structure in graphene provides the Dirac structure.

VII. ACKNOWLEDGEMENT

This work is supported by the NSFC (10974109 and 11174168), the SRFDP (20100002110079), and the 973 Program of China (2011CB606405). HCW was grateful to the SFI Short Term Travel fellowship support during his stay at PKU.

-
- [1] H. Mizuta and T. Tanoue, *The Physics and Applications of Resonant Tunneling Diodes*. Cambridge University Press, Cambridge, 1995.
 - [2] W. Middleton, M.E. Van Valkenburg, *Reference Data for Engineers: Radio, Electronics, Computers and Communications*. Boston Oxford, Newnes, 2002.
 - [3] A. Abdel-All, A. Elshafie, and M.M. Elhawary, *Vacuum* **59**, 845 (2000).
 - [4] J. McGinness, P. Corry, and P. Proctor, *Science* **183**, 853 (1974).
 - [5] H. Shirakawa, E.J. Louis, A.G. MacDiarmid, C.K. Chiang, and A.J. Heeger, *J. Chem. Soc., Chem. Commun.* 578 (1977).
 - [6] D. Dragoman and M. Dragoman, *Appl. Phys. Lett.* **90**, 143111 (2007).
 - [7] V. Nam Do, *Appl. Phys. Lett.* **92**, 216101 (2008).
 - [8] V. Nam Do, V. Hung Nguyen, P. Dollfus, and A. Bournel, *J. Appl. Phys.* **104**, 063708 (2008).
 - [9] Z.F. Wang, Q. Li, Q. W. Shi, X. Wang, J. Yang, J.G. Hou, and J. Chen, *Appl. Phys. Lett.* **92**, 133114 (2008).
 - [10] H. Ren, Q.-X. Li, Y. Luo, and J. Yang, *Appl. Phys. Lett.* **94**, 173110 (2009).
 - [11] H. Fang, R.-Z. Wang, S.-Y. Chen, M. Yan, X.-M. Song, and B. Wang, *Appl. Phys. Lett.* **98**, 082108 (2011).
 - [12] V. Nam Do and P. Dollfus, *J. Appl. Phys.* **107**, 063705 (2010).
 - [13] V. Hung Nguyen, A. Bournel, and P. Dollfus, *J. Appl. Phys.* **109**, 093706 (2011).
 - [14] V. Hung Nguyen, F. Mazzamuto, J. Saint-Martin, A. Bournel, and P. Dollfus, *Appl. Phys. Lett.* **99**, 042105 (2011).
 - [15] Gerson J. Ferreira, Michael N. Leuenberger, Daniel Loss, and J. Carlos Egues, *Phys. Rev. B* **84**, 125453 (2011).
 - [16] Y. Wu, D. B. Farmer, W. Zhu, S.-J. Han, C.D. Dimitrakopoulos, A. A. Bol, P. Avouris, and Y.-M. Lin, *ACS Nano* **6**, 2610 (2012).
 - [17] K. S. Novoselov, A. K. Geim, S. V. Morozov, D. Jiang, Y. Zhang, S. V. Dubonos, I. V. Grigorieva, and A. A. Firsov, *Science* **306**, 666 (2004).
 - [18] T.C.L.G. Sollner, W.D. Goodhue, P.E. Tannenwald, C.D. Parker, and D.D. Peck, *Appl. Phys. Lett.* **43**, 588 (1983); A.R. Bonnefoi, R.T. Collins, T.C. McGill, R.D. Burnham, and F.A. Ponce, *ibid.* **46**, 285 (1985).
 - [19] B. Huard, J. A. Sulpizio, N. Stander, K. Todd, B. Yang, and D. Goldhaber-Gordon, *Phys. Rev. Lett.* **98**, 236803 (2007); S. Russo, M. F. Craciun, M. Yamamoto, S. Tarucha, and A. F. Morpurgo, *New J. Phys.* **11**, 095018 (2009).
 - [20] J. Tworzydło, B. Trauzettel, M. Titov, A. Rycerz, and C.W.J. Beenakker, *Phys. Rev. Lett.* **96**, 246802 (2006).
 - [21] The kink effect is an interesting phenomena that the minimum differential conductance happens exactly at a bias equals to the Fermi energy and the operation window is the bias range between the current peak and valley points, where DC keeps negative.
 - [22] A. Javey, H. Kim, M. Brink, Q. Wang, A. Ural, J. Guo, P. McIntyre, P. Mceuen, M. Lundstrom, and H.J. Dai, *Nature Mater.* **1**, 241 (2002).
 - [23] Y. Song, H.C. Wu, and Y. Guo, *Appl. Phys. Lett.* **100**, 253116 (2012).
 - [24] Y.M. Blanter and M. Büttiker, *Phys. Rep.* **336**, 1 (2000).
 - [25] Y.-B. Tang, *et al.* *ACS Nano* **7**, 1970 (2012).
 - [26] Y. Song and Y. Guo, *J. Appl. Phys.* **109**, 104306 (2011).
 - [27] M. Born and E. Wolf, *Principles of optics: electromagnetic theory of propagation, interference and diffraction of light*. Oxford, Pergamon Press, 1964.
 - [28] I. Meric, M.Y. Han, A.F. Young, B. Ozyilmaz, P. Kim, and K.L. Shepard, *Nature Nanotech* **3**, 654 (2008).
 - [29] D. H. Chow and T. C. McGill, *Appl. Phys. Lett.* **48**, 1485 (1986); D. H. Chow, T. C. McGill, I. K. Sou, J. P. Faurie, and C. W. Nieh, *ibid.* **52**, 54 (1988).
 - [30] R. Beresford, L. F. Luo, and W. I. Wang, *Appl. Phys. Lett.* **54**, 1899 (1989); J. R. Söderström, D. H. Chow, and T. C. McGill, *ibid.* **55**, 1348 (1989).
 - [31] P.N. Racec, T. Stoica, C. Popescu, M. Lepsa, and Th. G. van de Roer, *Phys. Rev. B* **56**, 3595 (1997). Since the right barrier will be lower more than the left barrier under the bias, a right barrier with larger height or bigger width (i.e., positive λ_h or λ_w) should be excepted to obtain stronger NDR.
 - [32] X.L. Qi and S.C. Zhang, *Rev. Mod. Phys.* **83**, 1057 (2011).